(Received 26 January 2025, Accepted 25 April 2025, Scheduled 3 June 2025)

A Fast Electromagnetic Coupling Model Analysis Method for Modular Multi-High Frequency Switching Circuits

Rui Zhang[1,*], Yanfeng Gao[1], Jixuan Wang[1], and Han Meng[2]

[1]*School of Water Conservancy and Hydroelectric Power, Hebei University of Engineering, Handan 056038, China*
[2]*School of Mining and Geomatics Engineering, Hebei University of Engineering, Handan 056038, China*

ABSTRACT: In this paper, a fast electromagnetic coupling model analysis method is proposed to solve the challenging problems such as complex switching state, difficult electromagnetic modeling, and long parameter optimization process of multi-switch modular circuits with wide application prospects. In this method, a multi-loop circuit connected by multiple series-parallel high-speed switching devices is used as the research object, and each single loop can be regarded as a modular switching circuit for spatial electromagnetic coupling analysis. Considering the six complex states of the switching device, the speed and time change law $\mathrm{d}I/\mathrm{d}t$ of the multi-loop electromagnetic coupling and multi-switch switching state are simulated by using the circuit current change rate, and the circuit voltage fluctuation value $\mathrm{d}V$ is simplified to calculate the fast electromagnetic coupling model of the modular high-frequency switching circuit. By comparing with the electromagnetic coupling relationship calculated by the traditional Maxwell equations, the validity and rapidity of the fast electromagnetic coupling model are verified for the spatial electromagnetic field calculation of multi-switch modular circuit topology. By using the model analysis method, the optimal switching path with minimum power loss and maximum output efficiency can be predicted.

1. INTRODUCTION

With the mature development of high frequency switches, the modular application of multi-switch circuits has gradually increased and appeared in various electrical and electronic equipment and research fields. Examples include power electronic transformers, modular multilevel converters in DC systems, polyphase rectification, inverter systems, automotive power electronic circuits, transportation drive electrification systems, interconnection cables, and switching circuits for wide bandgap devices.

In the modular application of multi-switch circuits and the design of surrounding circuits, because there are multiple high-frequency switches, the on-off time of each switch will affect the spatial electromagnetic field of the circuit, which brings difficulties and challenges to the electromagnetic modeling accuracy, parameter optimization design, and real-time simulation research. In order to solve the influence of the increasing number of high-frequency switches on the electromagnetic field analysis of switching circuits, an electromagnetic coupling modeling method of multi-high-frequency switching circuits needs to be proposed.

At present, in the electromagnetic field research of multi-switch circuit application modules, there are fast multi-switch processing methods for parallel electromagnetic transient simulation and the establishment of real-time electromagnetic transient simulation system based on parallel [1]. However, this method mainly studies the electromagnetic simulation algorithm and does not consider the modular modeling for multi-switch circuits. The improved constant admittance method can be applied to the modeling of isolated dual active bridge DAB converter [2]. This modeling method is more efficient than the traditional electromagnetic transient (EMT) simulation, but it is not widely applicable to the modeling of other topology types of multi-switch circuits. With the wide application of the modular multilevel converter high voltage direct current system (MMC-HVDC), the multi-switch conducted electromagnetic interference model of auxiliary power supply (APS) has been proposed [3]. It is found that under the same input voltage, the common mode interference will increase with the increase of the number of series switches. However, the model is built with constraints and does not consider the number of parallel switches and the influence of switching circuit parameters on electromagnetic interference.

In order to simplify the difficulty of electromagnetic modeling caused by complex switching states, a fast, incomplete, and less computationally intensive electromagnetic model of switched reluctance motor was proposed [4]. The model uses an analytical model based on Maxwell equation, as well as interpolation and curve fitting techniques. The advantages of this method can also be perfected and optimized for electromagnetic modeling of multi-switch circuits. The selection of appropriate simplified modeling methods can significantly reduce the electromagnetic calculation time [5]. There are also some simplified electromagnetic models of switching circuits. Examples include frequency-domain electromagnetic compatibility (EMC) modeling techniques for three-phase inverter systems, conducted electromagnetic interference (EMI) models that consider switching states of different submodules, conducted EMI

* Corresponding author: Rui Zhang (ztlyaodi17@163.com).

modeling of actual switching waveforms of any 12-phase rectifier circuit based on state transitions, modular multilevel converter (MMC) adaptive models for electromagnetic transient simulation, and arbitrary topological voltage source changes based on switching state prediction Fast EMT simulation model of converter [6–11].

Due to the high switching speed of wide-band gap semiconductor devices, parasitic parameters will bring higher power loss and electromagnetic interference problems. At present, there are few researches on electromagnetic modeling of high-frequency switching circuits. On the one hand, the optimal layout mode of the package structure is optimized [12]. On the other hand, the complex electromagnetic state is rapidly optimized in the direction of mathematical calculation [13], and the equivalent circuit model can be established by time-domain and frequency-domain analysis methods [14, 15]. The switching sequence control law designed based on topological switching behavior has a positive impact on both slow scale and fast scale dynamics of power electronic systems [16]. For the electromagnetic system with complex switching state and layout structure at the same time, the electromagnetic model divided into several subsystems and sub-circuits can greatly simplify the difficulty of electromagnetic analysis of the system [17, 18].

In summary, the study of the fast simplified electromagnetic coupling model with multiple high-frequency switching circuit modules has important theoretical reference value for complex electromagnetic state analysis, system power loss prediction, feature topological dependence, and anti-electromagnetic interference. In this paper, a fast electromagnetic coupling model analysis method for modular high-frequency switching circuits is proposed to solve the problems of complex spatial electromagnetic coupling state, increased power loss, and serious electromagnetic interference caused by large number and high speed device switching action and circuit parameters around the device. In this method, a multi-loop circuit connected by multiple series-parallel high-speed switching devices is used as the research object, and each single loop can be regarded as a modular switching circuit for spatial electromagnetic coupling analysis. Under the complex action of series and parallel switching devices, the electromagnetic coupling relationship among multiple circuits is established by using Maxwell equations, and the mathematical law of the electromagnetic coupling of multiple circuits and the speed and time of the multi-switch state is explored. By using the model analysis method, the optimal switching path with minimum power loss and maximum output efficiency can be predicted.

2. THE SPATIAL ELECTROMAGNETIC COUPLING DISTRIBUTION OF MULTI-HIGH FREQUENCY SWITCHING CIRCUITS

In order to study the spatial electromagnetic coupling distribution characteristics around the multi-high-frequency switching circuit, this paper takes the modular high-frequency switching circuit as the research object. The switching circuit topology adopts multiple series-parallel high-frequency switches, and the position of each switch is shown in Figure 1. As shown in Figure 1, each switch has different operating times and speeds. By switching between multiple switches, a multi-loop structure can be constructed in the switching circuit, and the electromagnetic coupling relationship among the multiple loops can be established by using Maxwell's equations. Maxwell equations can be used to describe the electromagnetic coupling between complex circuits. Among them, the electromagnetic coupling relationship of each circuit is related to the spatial frequency of the circuit position, switching speed, time, and field parameters. On the contrary, problems such as circuit output power, output efficiency, and optimal switching path prediction can be optimized according to the electromagnetic coupling effect of each switch's action rate and time on multiple circuits [19, 20].

The double-circuit circuit composed of multiple switches in Figure 1 has two directional series-parallel circuit modes, and each construction mode has two circuits. Through the on-off and off-off action time and action rate of the series-parallel high-frequency switch, the spatial electromagnetic field coupling distribution around the modular high-frequency circuit is affected and determined.

There is a high-frequency switch at each branch position. The series spurious parameters L_{S12}, L_{S23}, $L_{S2'3'}$, $L_{S1'2'}$, $L_{S11'}$, $L_{S1'3}$, $L_{S22'}$, $L_{S2'3'}$ and parallel spurious parameters $L_{P11'}$, $L_{P22'}$, $L_{P33'}$, L_{P12}, $L_{P1'2'}$, $L_{P33'}$ are distributed around the switch. The different operating times of each switch t_{12}, t_{23}, $t_{33'}$, $t_{3'2'}$, $t_{2'1'}$, $t_{22'}$, $t_{2'3'}$, $t_{3'3}$ and speeds v_{12}, v_{23}, $v_{33'}$, $v_{3'2'}$, $v_{2'1'}$, $v_{22'}$, $v_{2'3'}$, $v_{3'3}$ affect the spatial electromagnetic field distribution around the double circuits. In Figure 1(a), when switches S_{12}, $S_{22'}$, $S_{2'1'}$ are switched on, current passes through loop l_1; when switches S_{12}, S_{23}, $S_{33'}$, $S_{3'2'}$, $S_{2'1'}$, $S_{22'}$ are switched on, there is current through loop

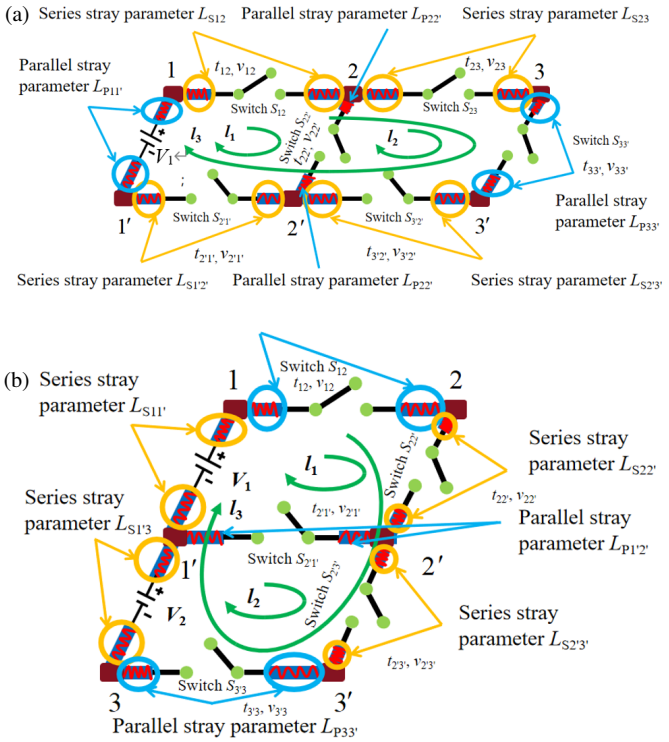

FIGURE 1. (a) Horizontal series and parallel double circuits. (b) Longitudinal series and parallel-double circuit.

l_2; when switches S_{12}, S_{23}, $S_{33'}$, $S_{3'2'}$, $S_{2'1'}$ are switched on, circuit l_3 has current through. Therefore, using the on-off and off-off of 6 switches, three different current motion states are constructed in the double circuits. In Figure 1(b), when switches S_{12}, $S_{22'}$, $S_{2'1'}$ are on, current passes through loop l_1; when switches S_{12}, $S_{22'}$, $S_{2'3'}$, $S_{3'3}$, $S_{2'1'}$ are on, there is current through the loop l_2; when switches S_{12}, $S_{22'}$, $S_{2'3'}$, $S_{3'3}$ are on, circuit l_3 has current through. Therefore, using 5 switches on and off, three different current motion states are constructed in the double circuits.

The complex electromagnetic coupling distribution of a single loop in space can be obtained by using the traditional Maxwell equations. When switches S_{12}, $S_{22'}$, $S_{2'1'}$ are switched on, current passes through loop l_1, and the spatial electromagnetic field distribution of single loop l_1 is shown in Figure 2.

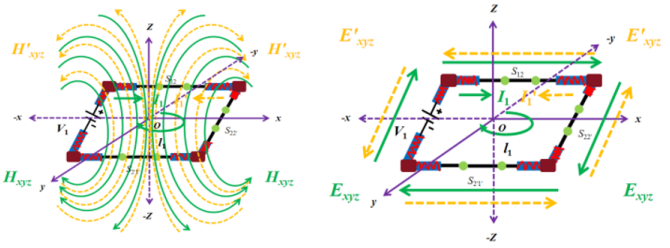

FIGURE 2. Spatial electromagnetic field distribution of single loop l_1.

In Figure 2, surrounding the single loop, on the left there is the magnetic field **H** distribution of the spatial electromagnetic field, and on the right there is the electric field **E** distribution of the spatial electromagnetic field. It can be seen that if the coordinate origin is set in the center of the loop, the magnetic field in the single loop is symmetrical radiation, and the distribution state is related to the loop radius length and loop x, y, and z coordinates. The electric field in the single circuit is edge-like, and its distribution is related to the x and y coordinates of the loop. Green and yellow indicate the current magnetic field $\mathbf{H}_{xyz}$, induced magnetic field $\mathbf{H}'_{xyz}$, electromotive force electric field $\mathbf{E}_{xyz}$, and induced electric field $\mathbf{E}'_{xyz}$, respectively. Due to the coupling of space electromagnetic field, there will be stray parameters on each side of the loop to produce voltage fluctuations at the end points.

Equation (1) of Maxwell's equations is used to establish the relationship between the space magnetic field **H** and electric field **E** and the radius length r, the loop x, y, z coordinates, and time t.

$$\begin{cases} \nabla \times \mathbf{H}(\mathbf{r},t) = \sigma \mathbf{E}(\mathbf{r},t) + \frac{\partial \varepsilon \mathbf{E}(\mathbf{r},t)}{\partial t} \\ \nabla \times \mathbf{E}(\mathbf{r},t) = -\frac{\partial \mu \mathbf{H}(\mathbf{r},t)}{\partial t} \\ \nabla \times \nabla \times \mathbf{E}(\mathbf{r},t) = -\sigma\mu \frac{\partial \mathbf{E}(\mathbf{r},t)}{\partial t} - \varepsilon\mu \frac{\partial^2 \mathbf{E}(\mathbf{r},t)}{\partial t^2} \\ \nabla \times \nabla \times \mathbf{H}(\mathbf{r},t) = -\sigma\mu \frac{\partial \mathbf{H}(\mathbf{r},t)}{\partial t} - \varepsilon\mu \frac{\partial^2 \mathbf{H}(\mathbf{r},t)}{\partial t^2} \end{cases} \quad (1)$$

There is also Equation (2) for calculating loop voltage ΔV and loop current ΔI. Considering the influence of spatially-coupled electromagnetic field around the loop on circuit parameters, Equation (3) for calculating voltage fluctuations is as follows:

$$\begin{cases} \oint_{l_1} \left(\mathbf{E}_x(\mathbf{r},s) + \mathbf{E}_y(\mathbf{r},s)\right) dl_1 = -\Delta V \\ \oint_l \mathbf{H}_z(\mathbf{r},s) dl = -\Delta I \end{cases} \quad (2)$$

$$\begin{cases} \Delta V_x(x,y,\beta) = \frac{2B_1}{\sigma} \frac{x^2}{(len2/2-|x|)} \cdot \frac{j\beta(|x|-len2/2)}{\sqrt{j\beta}r} \\ \qquad \sinh(\sqrt{j\beta}r) \\ \Delta V_y(x,y,\beta) = \frac{2B_1}{\sigma} \frac{y^2}{(len1/2-|y|)} \cdot \frac{j\beta(\text{ len }1/2-|y|)}{\sqrt{j\beta}r} \\ \qquad \sinh(\sqrt{j\beta}r) \end{cases} \quad (3)$$

It can be seen from Equation (3) that the voltage fluctuation obtained by the traditional calculation method is closely related to the actual coordinate parameters, the length *len*2, width *len*1 of the loop, and frequency ratio β. However, the traditional method has great limitations in calculation without detailed physical parameters. For the modular circuit topology with multiple switches, the switching state is complex, and the spatial electromagnetic field distribution under different switching states must be considered to find the optimal switching path, which minimizes the circuit loss and maximizes the output efficiency.

3. THE FAST ELECTROMAGNETIC COUPLING MODEL OF MULTI-HIGH FREQUENCY SWITCHING CIRCUIT

In the circuit topology with multiple high frequency switches, the spatial electromagnetic field distribution under different switching states is considered, and a fast electromagnetic coupling model is established in the complex switching state transformation. In this paper, a rectangular circuit is adopted as a general circuit topology. Except the left voltage source, the other three sides have a high-frequency switch, as shown in Figure 3. First, taking the horizontal series-parallel double-circuits as an example, there are 6 different switching states.

As can be seen from Figure 3, with the constant change of the switching state, the spatial electromagnetic field presents a lateral distribution, and the coupling effect can be transformed into the change of the flow direction of the induced current. The flow direction and size of the induced current are different in the six different switching states.

Switch state 1: When switch $S_{22'}$ changes from on to off, the loop current flow path changes from l_1 to $l_1 + l_2$, and the area of the electromagnetic field in the loop space also increases. The change of the switching state makes the induced electromagnetic field intermingled with the original spatial electromagnetic field. Because the current value I_1 changes to the current value I_2 after the switch is turned off instantaneously, the induced electromagnetic field of the loop l_1 is in the same direction as the original electromagnetic field, and the induced electromagnetic field of the loop l_2 is in the opposite direction as shown by the yellow dashed line.

Switch state 2: When switch $S_{33'}$ changes from off to on, the loop current flow path changes from l_1 to $l_1 + l_2$, and the electromagnetic field area in the loop space also increases. Because the current value I_1 changes to the current value $I_1 - I_3$ and I_3 after instantaneous switching, the induced electromagnetic field of the loop l_1 is in the same direction as the original

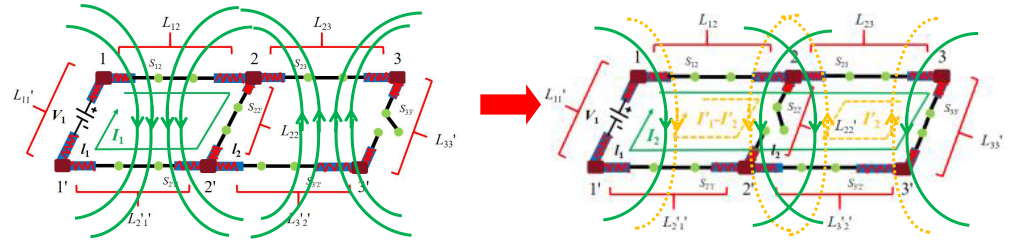

1) Switch status 1

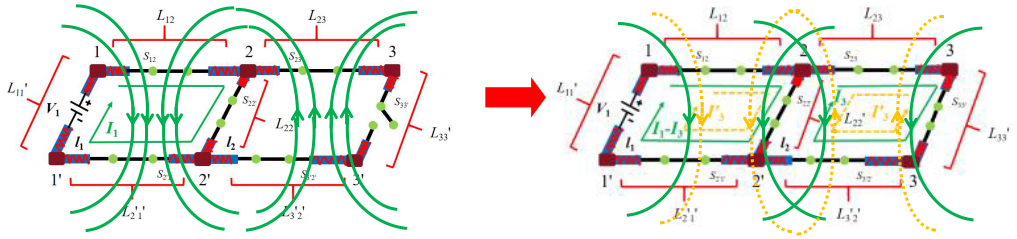

2) Switch status 2

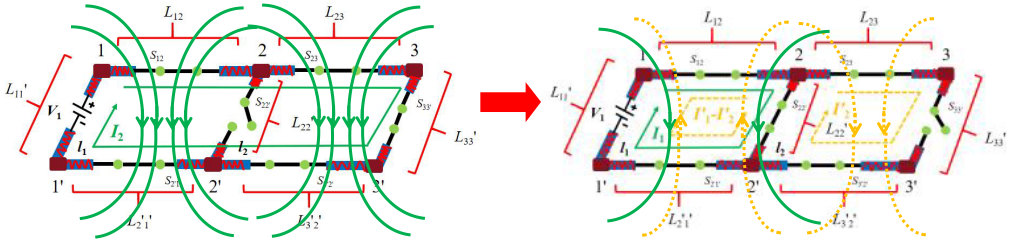

3) Switch status 3

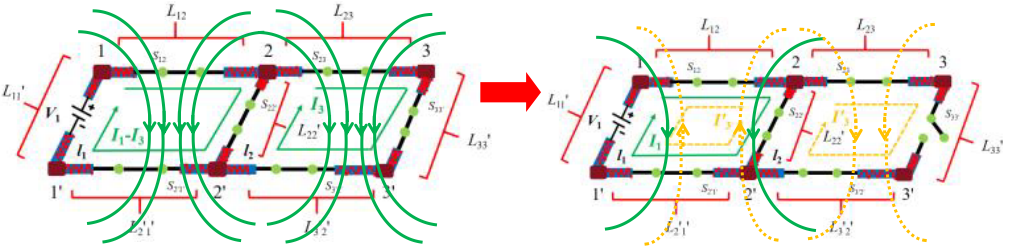

4) Switch status 4

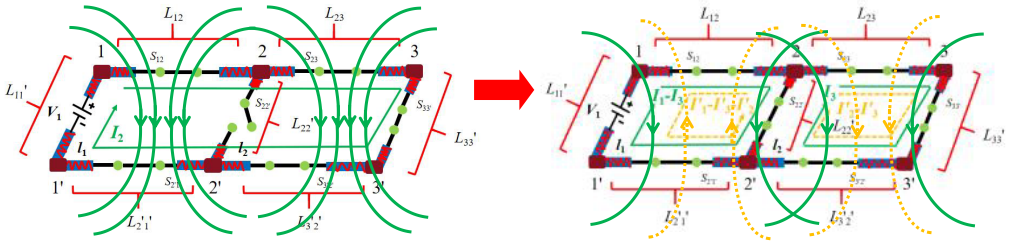

5) Switch status 5

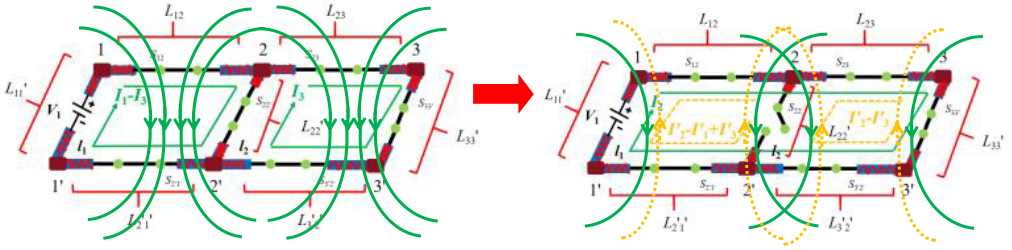

6) Switch status 6

FIGURE 3. Six switching states of horizontal series and parallel double circuits.

electromagnetic field, and the induced electromagnetic field of the loop l_2 is in the opposite direction.

Switch state 3: When switch $S_{22'}$ and $S_{33'}$ change from off and on to on and off, respectively, the circulation path of the loop current changes from $l_1 + l_2$ to l_1, and the area of the electromagnetic field in the loop space decreases accordingly. Because the current value I_2 changes to the current value I_1 after instantaneous switching and switching off, the induced electromagnetic field of the loop l_1 is opposite to the original electromagnetic field, and the newly added induced electromagnetic field of the loop l_2 is opposite to the induced electromagnetic field of the loop l_1.

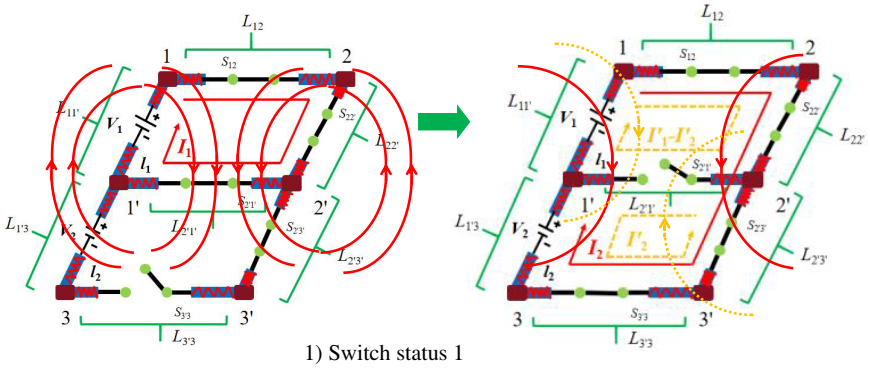

1) Switch status 1

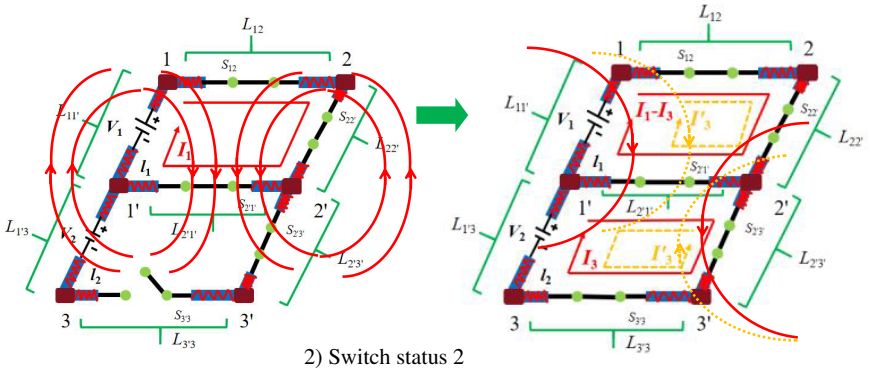

2) Switch status 2

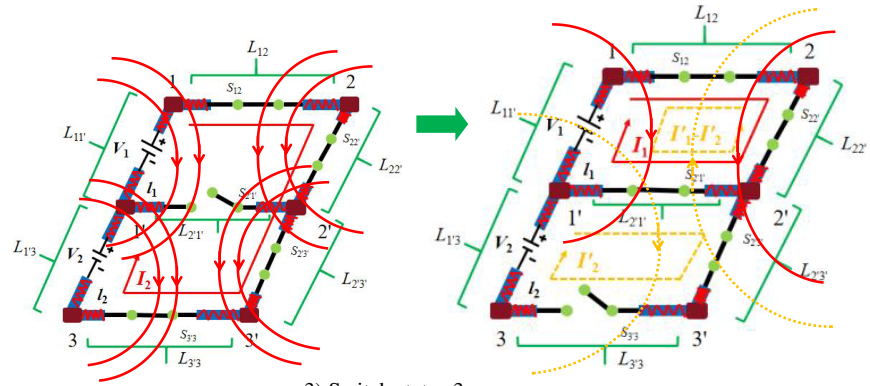

3) Switch status 3

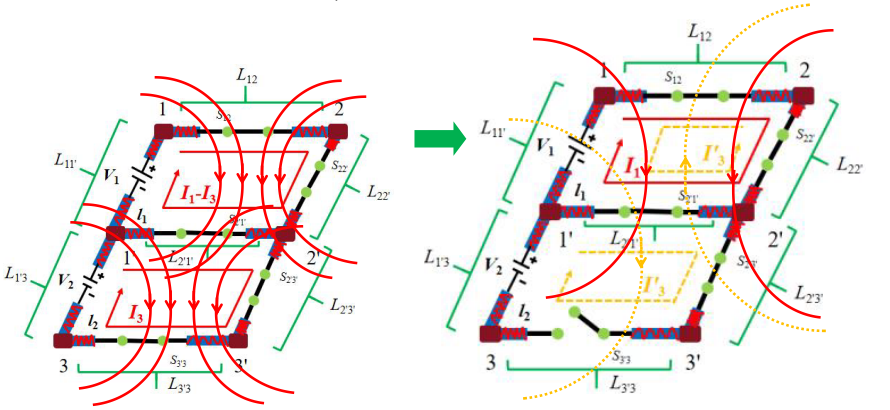

4) Switch status 4

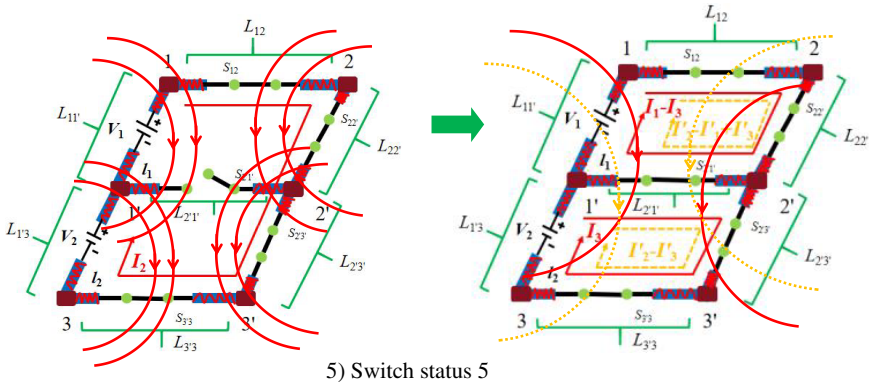

FIGURE 4. Six switching states of longitudinal series and parallel double circuit.

Switch state 4: When switch $S_{33'}$ changes from on to off, the loop current flow path changes from $l_1 + l_2$ to l_1, and the electromagnetic field area in the loop space decreases accordingly. Because the current value $I_1 - I_3$ and I_3 change to the current value I_1 after instantaneous switching and switching off, the induced electromagnetic field of the loop l_1 is opposite to the original electromagnetic field, and the newly added induced electromagnetic field of the loop l_2 is opposite to the induced electromagnetic field of the loop l_1.

Switch state 5: When switch $S_{22'}$ changes from off to on, the circulation area of loop current remains unchanged; the flow value changes from I_2 to $I_1 - I_3$ and I_3; the induced electromagnetic field of loop l_1 is opposite to the original electromagnetic field; and the newly added induced electromagnetic field of loop l_2 is opposite to the induced electromagnetic field of loop l_1.

Switch state 6: When switch $S_{22'}$ changes from on to off, the circulation area of loop current remains unchanged; the flow value changes from $I_1 - I_3$ and I_3 to I_2; the induced electromagnetic field of loop l_1 is opposite to the original electromagnetic field; and the newly added induced electromagnetic field of loop l_2 is in the same direction as the induced electromagnetic field of loop l_1. By analyzing the transition process of switching state 1→2→3→4→5→6 of the transverse series parallel circuit, it can be seen that the distribution direction, state and value of the transverse space electromagnetic field and induced electromagnetic field are closely related to the change of the loop current value, flow direction, and speed.

Next, taking the longitudinal series-parallel double-circuit as an example, there are also 6 different switching states.

The longitudinal series parallel loop has one more voltage source than the horizontal series parallel loop. The loop space coupling electromagnetic field is longitudinally distributed.

As can be seen from Figure 4, switch state 1: When switch $S_{3'3}$ and switch $S_{2'1'}$ change from off and on to on and off, respectively, the circulation path of the loop current changes from l_1 to $l_1 + l_2$, and the electromagnetic field area of the loop space also increases. Because the current value I_1 changes to the current value I_2 after instantaneous switching and switching off, the induced electromagnetic field of the loop l_1 is in the same direction as the original electromagnetic field, and the induced electromagnetic field of the loop l_2 is in the opposite direction.

Switch state 2: When switch $S_{3'3}$ changes from off to on, the loop current flow path changes from l_1 to $l_1 + l_2$, and the electromagnetic field area in the loop space also increases. Because the current value I_1 changes to the current value $I_1 - I_3$ and I_3 after instantaneous switching, the induced electromagnetic field of the loop l_1 is in the same direction as the original electromagnetic field, and the induced electromagnetic field of the loop l_2 is in the opposite direction.

Switch state 3: When switches $S_{21'}$ and $S_{3'3}$ change from off and on to on and off, respectively, the circulation path of the loop current changes from $l_1 + l_2$ to l_1, and the electromagnetic field area of the loop space decreases accordingly. Because the current value I_2 changes to the current value I_1 after instantaneous switching and switching off, the induced electromagnetic field of the loop l_1 is opposite to the original electromagnetic

field, and the newly added induced electromagnetic field of the loop l_2 is opposite to the induced electromagnetic field of the loop l_1.

Switch state 4: When switch $S_{3'3}$ changes from on to off, the loop current flow path changes from $l_1 + l_2$ to l_1, and the electromagnetic field area in the loop space decreases accordingly. Because the current value $I_1 - I_3$ and I_3 change to the current value I_1 after instantaneous switching off, the induced electromagnetic field of the loop l_1 is opposite to the original electromagnetic field, and the newly added induced electromagnetic field of the loop l_2 is opposite to the induced electromagnetic field of the loop l_1.

Switch state 5: When switch $S_{2'1'}$ changes from off to on, loop current flow area remains unchanged; flow value changes from I_2 to $I_1 - I_3$ and I_3; the induced electromagnetic field of loop l_1 is in the same direction as the original electromagnetic field; and the newly added induced electromagnetic field of loop l_2 is in the same direction as the induced electromagnetic field of loop l_1.

Switch state 6: When switch $S_{2'1'}$ changes from on to off, the circulation area of the loop current remains unchanged; the flow value changes from $I_1 - I_3$ and I_3 to I_2; the induced electromagnetic field of the loop l_1 is opposite to the original electromagnetic field; and the newly added induced electromagnetic field of the loop l_2 is in the same direction as the induced electromagnetic field of the loop l_1. By analyzing the transition process of switching state 1→2→3→4→5→6 of the longitudinal series parallel circuit, it can be seen that the distribution direction, state and value of the longitudinal space electromagnetic field and induced electromagnetic field are closely related to the loop current value, flow direction and speed.

To sum up, it is possible to use the change rate of loop current to simulate the electromagnetic coupling of multi-loop and the speed and time change law of multi-switch switching state, so that the fast electromagnetic coupling model of modular high-frequency switching circuit can be obtained, as shown in Equations (4), (5), (6), and (7).

$$\begin{cases} \frac{\mathrm{d}\left(I_1'-I_2'\right)}{\mathrm{d}t}=\frac{\mathrm{d}I_2'}{\mathrm{d}t},\quad \mathrm{d}I_1'=\mathrm{d}I_1,\quad \frac{\mathrm{d}I_1}{\mathrm{d}t}=\frac{\mathrm{d}I_2}{\mathrm{d}t} \\ \text{(Horizontal series-parallel circuit switch status 1)} \\ \frac{\mathrm{d}I_3}{\mathrm{d}t}=-\frac{\mathrm{d}I_3'}{\mathrm{d}t},\quad \frac{\mathrm{d}(I_1-I_3)}{\mathrm{d}t}+\frac{\mathrm{d}I_3}{\mathrm{d}t}=\frac{\mathrm{d}I_1}{\mathrm{d}t} \\ \text{(Horizontal series-parallel circuit switch status 2)} \\ \frac{\mathrm{d}\left(I_1'-I_2'\right)}{\mathrm{d}t}=\frac{\mathrm{d}I_2'}{\mathrm{d}t},\quad \mathrm{d}I_1'=\mathrm{d}I_1,\quad \frac{\mathrm{d}I_1}{\mathrm{d}t}=\frac{\mathrm{d}I_2}{\mathrm{d}t} \\ \text{(Horizontal series-parallel circuit switch status 3)} \\ \frac{\mathrm{d}I_3}{\mathrm{d}t}=-\frac{\mathrm{d}I_3'}{\mathrm{d}t},\quad \frac{\mathrm{d}I_1}{\mathrm{d}t}+\frac{\mathrm{d}I_3'}{\mathrm{d}t}=\frac{\mathrm{d}(I_1-I_3)}{\mathrm{d}t} \\ \text{(Horizontal series-parallel circuit switch status 4)} \\ \frac{\mathrm{d}\left(I_1'-I_3'-I_2'\right)}{\mathrm{d}t}=\frac{\mathrm{d}\left(I_2'-I_3'\right)}{\mathrm{d}t},\quad \frac{\mathrm{d}(I_1-I_3)}{\mathrm{d}t}+\frac{\mathrm{d}I_3}{\mathrm{d}t}=\frac{\mathrm{d}I_2}{\mathrm{d}t} \\ \text{(Horizontal series-parallel circuit switch status 5)} \\ \frac{\mathrm{d}\left(I_2'-I_1'+I_3'\right)}{\mathrm{d}t}=\frac{\mathrm{d}\left(I_2'-I_3'\right)}{\mathrm{d}t},\quad \frac{\mathrm{d}(I_1-I_3)}{\mathrm{d}t}+\frac{\mathrm{d}I_3}{\mathrm{d}t}=\frac{\mathrm{d}I_2}{\mathrm{d}t} \\ \text{(Horizontal series-parallel circuit switch status 6)} \\ \oint_l \mathbf{H}_z(\mathbf{r},s)dl=-\mathrm{d}I\ (I=I_1'-I_2',I_1,I_1',I_2,I_2',I_3, \\ I_3',I_1-I_3,I_2'-I_3',I_1'-I_3'-I_2',I_2'-I_1'+I_3') \end{cases} \tag{4}$$

$$\begin{cases} \frac{\mathrm{d}\left(I_1'-I_2'\right)}{\mathrm{d}t}=\frac{\mathrm{d}I_2'}{\mathrm{d}t},\quad \mathrm{d}I_1'=\mathrm{d}I_1,\quad \frac{\mathrm{d}I_1}{\mathrm{d}t}=\frac{\mathrm{d}I_2}{\mathrm{d}t} \\ \text{(Longitudinal series-parallel circuit switch status 1)} \\ \frac{\mathrm{d}I_3}{\mathrm{d}t}=-\frac{\mathrm{d}I_3'}{\mathrm{d}t},\quad \frac{\mathrm{d}(I_1-I_3)}{\mathrm{d}t}+\frac{\mathrm{d}I_3}{\mathrm{d}t}=\frac{\mathrm{d}I_1}{\mathrm{d}t} \\ \text{(Longitudinal series-parallel circuit switch status 2)} \\ \frac{\mathrm{d}\left(I_1'-I_2'\right)}{\mathrm{d}t}=\frac{\mathrm{d}I_2'}{\mathrm{d}t},\quad \mathrm{d}I_1'=\mathrm{d}I_1,\quad \frac{\mathrm{d}I_1}{\mathrm{d}t}=\frac{\mathrm{d}I_2}{\mathrm{d}t} \\ \text{(Longitudinal series-parallel circuit switch status 3)} \\ \frac{\mathrm{d}I_3}{\mathrm{d}t}=-\frac{\mathrm{d}I_3'}{\mathrm{d}t},\quad \frac{\mathrm{d}I_1}{\mathrm{d}t}+\frac{\mathrm{d}I_3'}{\mathrm{d}t}=\frac{\mathrm{d}(I_1-I_3)}{\mathrm{d}t} \\ \text{(Longitudinal series-parallel circuit switch status 4)} \\ \frac{\mathrm{d}\left(I_2'-I_1'+I_3'\right)}{\mathrm{d}t}=\frac{\mathrm{d}\left(I_2'-I_3'\right)}{\mathrm{d}t},\quad \frac{\mathrm{d}(I_1-I_3)}{\mathrm{d}t}+\frac{\mathrm{d}I_3}{\mathrm{d}t}=\frac{\mathrm{d}I_2}{\mathrm{d}t} \\ \text{(Longitudinal series-parallel circuit switch status 5)} \\ \frac{\mathrm{d}\left(I_2'-I_1'+I_3'\right)}{\mathrm{d}t}=\frac{\mathrm{d}\left(I_2'-I_3'\right)}{\mathrm{d}t},\quad \frac{\mathrm{d}(I_1-I_3)}{\mathrm{d}t}+\frac{\mathrm{d}I_3}{\mathrm{d}t}=\frac{\mathrm{d}I_2}{\mathrm{d}t} \\ \text{(Longitudinal series-parallel circuit switch status 6)} \\ \oint_l \mathbf{H}_z(\mathbf{r},s)dl=-\mathrm{d}I\ (I=I_1'-I_2',I_1,I_1',I_2,I_2',I_3, \\ I_3',I_1-I_3,I_2'-I_3',I_2'-I_1'+I_3',I_2'-I_1'+I_3') \end{cases} \tag{5}$$

$$\begin{cases} \mathrm{d}V=(L_{12}+L_{23}+L_{33'}+L_{3'2'}+L_{2'1'}+L_{11'})\frac{\mathrm{d}I_2}{\mathrm{d}t} \\ \quad +(L_{12}+L_{22'}+L_{2'1'}+L_{11'})\frac{\mathrm{d}(I_1'-I_2')}{\mathrm{d}t} \\ \quad -(L_{23}+L_{22'}+L_{33'}+L_{3'2'})\frac{\mathrm{d}I_2'}{\mathrm{d}t} \\ \text{(Horizontal series-parallel circuit switch status 1)} \\ \mathrm{d}V=(L_{12}+L_{22'}+L_{2'1'}+L_{11'})\frac{\mathrm{d}(I_1-I_3)}{\mathrm{d}t} \\ \quad +(L_{12}+L_{22'}+L_{2'1'}+L_{11'})\frac{\mathrm{d}I_3'}{\mathrm{d}t} \\ \quad +(L_{23}+L_{22'}+L_{33'}+L_{3'2'})\frac{\mathrm{d}I_3}{\mathrm{d}t} \\ \quad -(L_{23}+L_{22'}+L_{33'}+L_{3'2'})\frac{\mathrm{d}I_3'}{\mathrm{d}t} \\ \text{(Horizontal series-parallel circuit switch status 2)} \\ \mathrm{d}V=(L_{12}+L_{22'}+L_{2'1'}+L_{11'})\frac{\mathrm{d}I_1}{\mathrm{d}t} \\ \quad +(L_{23}+L_{22'}+L_{33'}+L_{3'2'})\frac{\mathrm{d}I_2'}{\mathrm{d}t} \\ \quad -(L_{12}+L_{22'}+L_{2'1'}+L_{11'})\frac{\mathrm{d}\left(I_1'-I_2'\right)}{\mathrm{d}t} \\ \text{(Horizontal series-parallel circuit switch status 3)} \\ \mathrm{d}V=(L_{12}+L_{22'}+L_{2'1'}+L_{11'})\frac{\mathrm{d}I_1}{\mathrm{d}t} \\ \quad +(L_{23}+L_{22'}+L_{33'}+L_{3'2'})\frac{\mathrm{d}I_3'}{\mathrm{d}t} \\ \quad -(L_{12}+L_{22'}+L_{2'1'}+L_{11'})\frac{\mathrm{d}I_3'}{\mathrm{d}t} \\ \text{(Horizontal series-parallel circuit switch status 4)} \\ \mathrm{d}V=(L_{12}+L_{22'}+L_{2'1'}+L_{11'})\frac{\mathrm{d}(I_1-I_3)}{\mathrm{d}t} \\ \quad +(L_{23}+L_{22'}+L_{33'}+L_{3'2'})\frac{\mathrm{d}I_3}{\mathrm{d}t} \\ \quad +(L_{23}+L_{22'}+L_{33'}+L_{3'2'})\frac{\mathrm{d}\left(I_2'-I_3'\right)}{\mathrm{d}t} \\ \quad -(L_{12}+L_{22'}+L_{2'1'}+L_{11'})\frac{\mathrm{d}\left(I_1'-I_3'-I_2'\right)}{\mathrm{d}t} \\ \text{(Horizontal series-parallel circuit switch status 5)} \\ \mathrm{d}V=(L_{12}+L_{23}+L_{33'}+L_{3'2'}+L_{2'1'}+L_{11'})\frac{\mathrm{d}I_2}{\mathrm{d}t} \\ \quad -(L_{12}+L_{22'}+L_{2'1'}+L_{11'})\frac{\mathrm{d}(I_2'-I_1'+I_3')}{\mathrm{d}t} \\ \quad -(L_{23}+L_{22'}+L_{33'}+L_{3'2'})\frac{\mathrm{d}\left(I_2'-I_3'\right)}{\mathrm{d}t} \\ \text{(Horizontal series-parallel circuit switch status 6)} \\ \oint_{l_1}\left(\mathbf{E}_x(\mathbf{r},s)+\mathbf{E}_y(\mathbf{r},s)\right)dl=-\mathrm{d}V \end{cases} \tag{6}$$

$$
\begin{cases}
\mathrm{d}V = (L_{12}+L_{22'}+L_{2'3'}+L_{3'3}+L_{1'3}+L_{11'})\frac{\mathrm{d}I_2}{\mathrm{d}t} \\
\quad +(L_{12}+L_{22'}+L_{2'1'}+L_{11'})\frac{\mathrm{d}(I_1'-I_2')}{\mathrm{d}t} \\
\quad -(L_{1'3}+L_{2'1'}+L_{3'3}+L_{2'3'})\frac{\mathrm{d}I_2'}{\mathrm{d}t} \\
\text{(Longitudinal series-parallel circuit switch status 1)} \\
\mathrm{d}V = (L_{12}+L_{22'}+L_{2'1'}+L_{11'})\frac{\mathrm{d}(I_1-I_3)}{\mathrm{d}t} \\
\quad +(L_{12}+L_{22'}+L_{2'1'}+L_{11'})\frac{\mathrm{d}I_3'}{\mathrm{d}t} \\
\quad +(L_{2'1'}+L_{2'3'}+L_{3'3}+L_{1'3})\frac{\mathrm{d}I_3}{\mathrm{d}t} \\
\quad -(L_{2'1'}+L_{2'3'}+L_{3'3}+L_{1'3})\frac{\mathrm{d}I_3'}{\mathrm{d}t} \\
\text{(Longitudinal series-parallel circuit switch status 2)} \\
\mathrm{d}V = (L_{12}+L_{22'}+L_{2'1'}+L_{11'})\frac{\mathrm{d}I_1}{\mathrm{d}t} \\
\quad +(L_{2'1'}+L_{2'3'}+L_{3'3}+L_{1'3})\frac{\mathrm{d}I_2'}{\mathrm{d}t} \\
\quad -(L_{12}+L_{22'}+L_{2'1'}+L_{11'})\frac{\mathrm{d}(I_1'-I_2')}{\mathrm{d}t} \\
\text{(Langitudimal series-parallel circuit switch status 3)} \\
\mathrm{d}V = (L_{12}+L_{22'}+L_{2'1'}+L_{11'})\frac{\mathrm{d}I_1}{\mathrm{d}t} \\
\quad +(L_{2'1'}+L_{2'3'}+L_{3'3}+L_{1'3})\frac{\mathrm{d}I_3'}{\mathrm{d}t} \\
\quad -(L_{12}+L_{22'}+L_{2'1'}+L_{11'})\frac{\mathrm{d}I_3'}{\mathrm{d}t} \\
\text{(Longitudinal series-parallel circuit switch status 4)} \\
\mathrm{d}V = (L_{12}+L_{22'}+L_{2'1'}+L_{11'})\frac{\mathrm{d}(I_1-I_3)}{\mathrm{d}t} \\
\quad +(L_{2'1'}+L_{2'3'}+L_{3'3}+L_{1'3})\frac{\mathrm{d}I_3}{\mathrm{d}t} \\
\quad +(L_{12}+L_{22'}+L_{2'1'}+L_{11'})\frac{\mathrm{d}(I_2'-I_1'+I_3')}{\mathrm{d}t} \\
\quad +(L_{2'1'}+L_{2'3'}+L_{3'3}+L_{1'3})\frac{\mathrm{d}(I_2'-I_3')}{\mathrm{d}t} \\
\text{(Longitudinal series-parallel circuit switch status 5)} \\
\mathrm{d}V = (L_{12}+L_{22'}+L_{2'3'}+L_{3'3}+L_{1'3}+L_{11'})\frac{\mathrm{d}I_2}{\mathrm{d}t} \\
\quad -(L_{12}+L_{22'}+L_{2'1'}+L_{11'})\frac{\mathrm{d}(I_2'-I_1'+I_3')}{\mathrm{d}t} \\
\quad -(L_{2'1'}+L_{2'3'}+L_{3'3}+L_{1'3})\frac{\mathrm{d}(I_2'-I_3')}{\mathrm{d}t} \\
\text{(Longitudinal series-parallel circuit switch status 6)} \\
\oint_{l_1}(\mathbf{E}_x(\mathbf{r},s)+\mathbf{E}_y(\mathbf{r},s))\,dl = -\mathrm{d}V
\end{cases}
\tag{7}
$$

The process of voltage fluctuation calculated according to the fast electromagnetic coupling model of Equation (6) and Equation (7) is also greatly simplified. The following is a detailed comparison with the traditional electromagnetic coupling calculation method to verify the effectiveness and rapidity of the fast electromagnetic coupling model for the spatial electromagnetic field calculation of the multi-switch modular circuit topology. Considering and analyzing the spatial electromagnetic field distribution under different switching states, the optimal switching path is found to minimize the circuit loss and maximize the output efficiency.

4. SIMULATION ANALYSIS

The simulation data of the fast electromagnetic coupling model is compared with the traditional electromagnetic coupling calculation method, and the current rate, voltage fluctuation, and efficiency are verified in a certain data segment.

It can be seen from Figure 5 that the fast electromagnetic coupling model can accurately describe the voltage fluctuation and current change rate under the spatial electromagnetic coupling state. The curves showed a symmetrical upward and downward trend. Compared with the traditional electromagnetic field calculation method, the prediction curve of the fast electromagnetic coupling model is inside the traditional electromagnetic field value change curve, which verifies the effectiveness and rapidity of the fast electromagnetic coupling model.

As can be seen from Figure 6, the fast electromagnetic coupling model is faster and more accurate than the traditional electromagnetic field calculation methods in the topology space of multi-switch module circuits. The spatial electromagnetic field distribution under different switching states is considered and analyzed, and the optimal switching path with minimum circuit loss and maximum output efficiency is found. By comparing the data of the two methods, it can be seen that the results of the rapid electromagnetic coupling model analysis method are

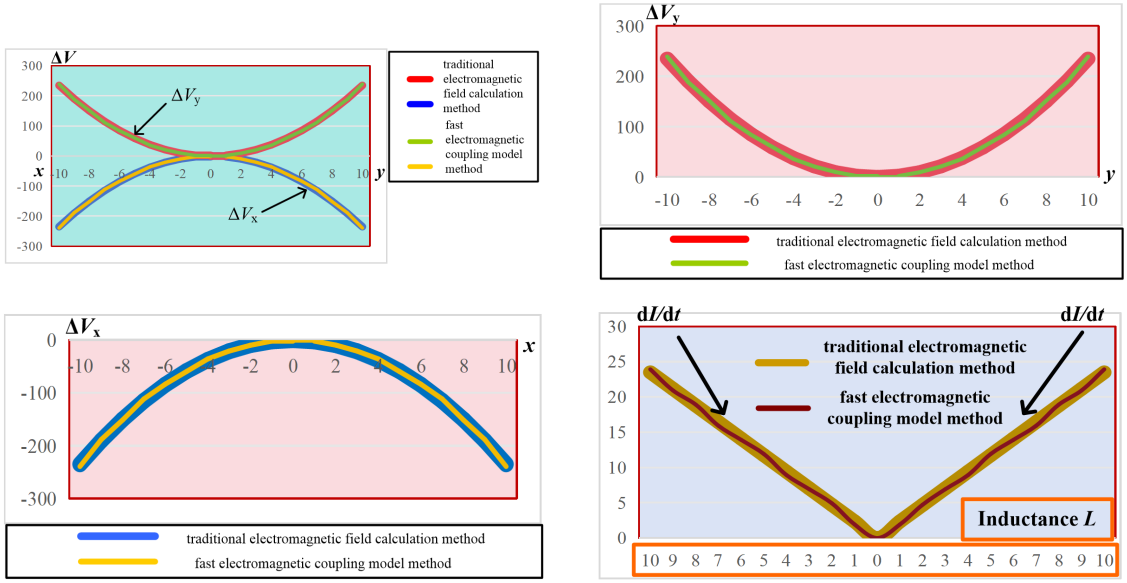

FIGURE 5. Comparison between fast electromagnetic coupling model and traditional electromagnetic field calculation method.

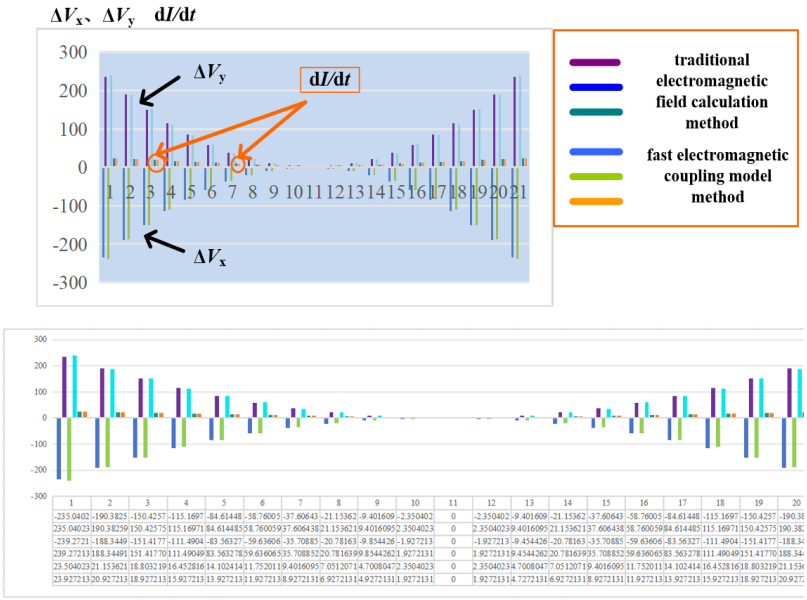

FIGURE 6. The numerical comparison of voltage fluctuation ΔV_x, ΔV_y and current change rate $\mathrm{d}I/\mathrm{d}t$ under two methods.

similar to those of the traditional electromagnetic calculation method, with very small errors.

5. CONCLUSION

In this paper, modeling and analysis of spatially coupled electromagnetic fields are carried out in horizontal and longitudinal multiswitch circuit topologies. By exploring the relationship among complex switching state, current flow direction, speed, and spatial electromagnetic field distribution of modular switching circuit, the mathematical equation of theoretical logic relationship is further obtained. By using this fast mathematical calculation method, the current flow rate and voltage fluctuation caused by the coupling electromagnetic field in the loop topological space under the complex switching state can be calculated numerically. Through the calculation results of the equation, the current utilization efficiency of each branch in the circuit can be quickly obtained, and the optimal switching path and maximum efficiency of the whole circuit can be obtained. Since the fast electromagnetic coupling analysis method proposed in this paper utilizes the different conduction and turn-off moments of multiple switches to perform switch actions and optimize the current flow path, it is suitable for the rapid optimization of modular circuit models under the coupling influence of complex electromagnetic relationships. On the contrary, it is not applicable when the number of high-frequency switching devices, parameters, and circuit loops are relatively small. Therefore, in the application process of the rapid electromagnetic coupling model analysis method, it is necessary to conduct optimization analysis for the specific working conditions that actually occur.

ACKNOWLEDGEMENT

This paper is supported by Natural Science Foundation project of Hebei Province E2024402072 and Scientific Research (Youth Top) project of higher Education Department of Hebei Province BJ2025031.

REFERENCES

[1] Gong, Y., L. Chen, Y. Chen, and Y. Xu, "A parallel based real-time electromagnetic transient simulator for IPS," in *2011 IEEE Electric Ship Technologies Symposium*, 96–101, Alexandria, VA, USA, 2011.

[2] Gong, W. M., Z. Zhu, S. K. Xu, and C. Wang, "Modeling and electromagnetic transient (EMT) simulation of a dual active bridge DC-DC converter," in *2019 10th International Conference on Power Electronics and ECCE Asia (ICPE 2019 — ECCE Asia)*, 2199–2204, Busan, Korea (South), 2019.

[3] Chen, X., W. Chen, Y. Han, Y. Sha, X. Yang, and X. Li, "Common-mode interference study of a auxiliary power supply based on the serialization of SiC MOSFETs for MMC-HVDC system," in *2016 IEEE 8th International Power Electronics and Motion Control Conference (IPEMC-ECCE Asia)*, 31–36, Hefei, China, 2016.

[4] Watthewaduge, G., E. Sayed, A. Emadi, and B. Bilgin, "Electromagnetic modeling techniques for switched reluctance machines: State-of-the-art review," *IEEE Open Journal of the Industrial Electronics Society*, Vol. 1, 218–234, 2020.

[5] Sano, K., S. Horiuchi, and T. Noda, "Comparison and selection of grid-tied inverter models for accurate and efficient EMT simulations," *IEEE Transactions on Power Electronics*, Vol. 37, No. 3, 3462–3472, Mar. 2022.

[6] Zhou, W., X. Pei, Y. Xiang, and Y. Kang, "A new EMI modeling method for mixed-mode noise analysis in three-phase inverter system," *IEEE Access*, Vol. 8, 71 535–71 547, 2020.

[7] Sun, T., X. Pei, Y. Shan, J. Pei, and D. Jiang, "Submodule switching-state based EMI modeling and mixed-mode EMI phenomenon in MMC," *IEEE Transactions on Power Electronics*, Vol. 38, No. 2, 1831–1843, Feb. 2023.

[8] Xu, Y., Q.-F. Liu, B. Mou, C. Huang, W. Peng, X. Zhu, and H.-Q. Zhang, "A modeling method and characteristics study of EMI in 12-phase rectifier circuit with actual switching process based on state transition," *IEEE Transactions on Electromagnetic Com-*

patibility, Vol. 66, No. 3, 1001–1014, Jun. 2024.

[9] Xu, Y., C. N. M. Ho, A. Ghosh, and D. Muthumuni, "An electrical transient model of IGBT-diode switching cell for power semiconductor loss estimation in electromagnetic transient simulation," *IEEE Transactions on Power Electronics*, Vol. 35, No. 3, 2979–2989, Mar. 2020.

[10] Stepanov, A., J. Mahseredjian, U. Karaagac, and H. Saad, "Adaptive modular multilevel converter model for electromagnetic transient simulations," *IEEE Transactions on Power Delivery*, Vol. 36, No. 2, 803–813, Apr. 2021.

[11] Gao, S., Y. Song, Y. Chen, Z. Yu, and R. Zhang, "Fast simulation model of voltage source converters with arbitrary topology using switch-state prediction," *IEEE Transactions on Power Electronics*, Vol. 37, No. 10, 12 167–12 181, Oct. 2022.

[12] Zhang, Y., Y. Xie, C. Chen, X. Guo, Y. Yan, L. Yang, and Y. Kang, "Comprehensive analysis and optimization of parasitic capacitance on conducted EMI and switching losses in hybrid-packaged SiC power modules," *IEEE Transactions on Power Electronics*, Vol. 38, No. 11, 13 988–14 003, Nov. 2023.

[13] Zhang, R., W. Chen, Y. Zhou, Z. Shi, R. Yan, and X. Yang, "Mathematical modeling of EMI spectrum envelope based on switching transient behavior," *IEEE Journal of Emerging and Selected Topics in Power Electronics*, Vol. 10, No. 2, 2497–2515, Apr. 2022.

[14] Kharanaq, F. A., A. Emadi, and B. Bilgin, "Modeling of conducted emissions for EMI analysis of power converters: State-of-the-art review," *IEEE Access*, Vol. 8, 189 313–189 325, 2020.

[15] Ye, H., F. Gao, W. Pei, and L. Kong, "Wave function and multi-scale modeling of MMC-HVdc system for wide-frequency transient simulation," *IEEE Journal of Emerging and Selected Topics in Power Electronics*, Vol. 9, No. 5, 5906–5917, Oct. 2021.

[16] Chatterjee, D. and S. K. Mazumder, "EMI mitigation of a Ćuk-based power-electronic system using switching-sequence-based control," *IEEE Transactions on Power Electronics*, Vol. 36, No. 9, 10 627–10 644, Sep. 2021.

[17] Zhu, R., T. Liang, V. Dinavahi, and G. Liang, "Wideband modeling of power SiC mosfet module and conducted EMI prediction of MVDC railway electrification system," *IEEE Transactions on Electromagnetic Compatibility*, Vol. 62, No. 6, 2621–2633, Dec. 2020.

[18] Zhu, R., N. Lin, V. Dinavahi, and G. Liang, "An accurate and fast method for conducted EMI modeling and simulation of MMC-based HVdc converter station," *IEEE Transactions on Power Electronics*, Vol. 35, No. 5, 4689–4702, May 2020.

[19] Zhang, R., Y. Wang, and H. Xu, "A novel analytical method suitable for coupled electromagnetic field of circuit," *Progress In Electromagnetics Research M*, Vol. 100, 35–50, 2020.

[20] Zhang, R., Y. Gao, and J. Wang, "A spatial electromagnetic field analysis method for estimating the dynamic positions of multiple mobile high-frequency power supplies," *Progress In Electromagnetics Research C*, Vol. 145, 9–20, 2024.